A CONSISTENCY ANALYSIS OF LEAF AREA INDEX RETRIEVAL FROM OVERLAPPING CLEAR-SKY LANDSAT ETM+ IMAGERY

Chris Butson†
Richard Fernandes‡

†Prologic Consulting
75 Albert Street, Suite 206
Ottawa, Ontario Canada
K1P 5E7

‡Natural Resources Canada
Canada Centre for Remote Sensing
588 Booth St. Ottawa, Ontario
Canada
K1A 0Y7

E-mail: Chris.Butson@ccrs.nrcan.gc.ca

Abstract

In this study, the consistency of systematic retrievals of surface reflectance and leaf area index was assessed using overlap regions in adjacent Landsat ETM+ scenes. Adjacent scenes were acquired within 7 to 25 days apart to minimize variations in the land surface reflectance between acquisition dates. Each Landsat ETM+ scene was independently geo-referenced and atmospherically corrected using a variety of standard approaches. Leaf area index (LAI) models were then applied to the surface reflectance data and the difference in LAI between overlapping scenes was evaluated. The results from this analysis show that systematic LAI retrieval from Landsat ETM+ imagery using a baseline atmospheric correction approach that assumes a constant aerosol optical depth equal to 0.06 is consistent to within ±0.61 LAI units. The average absolute difference in

LAI retrieval over all ten image pairs was 26% for a mean LAI of 2.05 and the maximum absolute difference over any one pair was 61% for a mean LAI of 1.13. When no atmospheric correction was performed on the data, the consistency in LAI retrieval was improved by 1%. When a scene-based dense, dark vegetation atmospheric correction algorithm was used, the LAI retrieval differences became 3% worse than the baseline correction. This implies that a scene-based atmospheric correction procedure may improve the absolute accuracy of LAI retrieval without having a major impact on retrieval consistency. Such consistency trials provide insight into the current limits concerning surface reflectance and LAI retrieval from fine spatial resolution remote sensing imagery with respect to the variability in clear-sky atmospheric conditions.

1.0 Introduction

Leaf area index (LAI) is defined as half the all-sided green leaf area per unit ground surface area projected on the horizontal datum (United Nations FAO). It is a quantitative indicator of foliage density and has been used for monitoring vegetation status (Cayrol et al., 2000; Waring and Running, 1998), modelling fluxes of water (Su, 2000; Nouvellon et al., 2000), energy (Bonan, 1995) and greenhouse gases (Liu et al., 1997; Coops et al., 2001) between the biosphere and atmosphere. LAI has been an important variable in the progression of national (Chen et al., 2002; Fernandes et al., in press) and international initiatives (Sellers et al., 1994; Myneni et al., 1997) for the monitoring of forest vegetation using space-borne satellite sensors. Currently, there is a growing need for quality assured data products as inputs into continental and global data assimilation strategies (Cohen and Justice, 1999; Houser and Cosgrove, 2002). With the increased availability of well-calibrated Landsat Enhanced Thematic Mapper-Plus (ETM+, or for simplicity in this paper TM) imagery, consistent processing methods are in demand for systematic and repeatable monitoring of vegetation productivity using such data (Wood

et al., 2002). Moreover, the accuracy and precision errors of the derived products should be known since these data are often used as inputs into calibration and validation of coarser scale products (Fernandes et al., in press). In this paper, we consider accuracy to represent how well the calculated LAI values match the actual values obtained from field measurement (Goodchild, 2000, pg. 7). The measurement of accuracy is difficult in the practical sense, since methods for LAI measurement using field and remote sensing-based approaches are not universal or standardized between researchers. Furthermore, we were not able to obtain spatial and temporal field-based measurements of LAI coincident with the overlap regions analyzed in this study. As a result, the accuracy of LAI retrieval from TM imagery will not be addressed in this research. What we do focus on in this study is the statistical precision of LAI retrieval from TM imagery. For the purposes of this research, we define the general term 'precision' as the fineness of the measurement increment, or a measure of how consistent estimates of a particular variable can be derived through a specified data processing chain. This definition can be decomposed into two distinct parts to address the difference between numerical and statistical precision. The former is usually found in the discipline of computer science to describe "the exactness, or degree of detail with which an individual observation is measured (e.g. 'double precision floating point numbers)" (Mowrer and Congalton, 2000, pg. xvi). Alternatively, Marriott (1990) describes the dispersion of repeated observations about their own mean as statistical precision. Repeatedly estimating a parameter such as surface reflectance or LAI and deriving the variability in these collective estimates will approximate the statistical precision. We use the term consistency as opposed to precision in this paper as it reflects a broadly defined precision estimate. A true value of precision would be the standard deviation in a collection of values acquired in the same overlap region. Since we only use two samples within a region of overlapping TM coverage, the consistency reflects the degree of reliability between these two measurements with which surface reflectance and LAI can be approximated from remote sensing data. Since surface reflectance is the fundamental parameter for deriving LAI, we feel that a measure of consistency should be determined and be traceable throughout the entire data processing chain.

The processing chain to generate an LAI product from TM imagery is:

(1) radiometric calibration of raw data ;
(2) atmospheric / BRDF correction to translate TOA reflectance to top-of-canopy bi-directional reflectance; and,
(3) application of algorithms to calculate LAI from reflectance (including screening for cloud, haze, land cover and land use patterns).

Although these procedures are not difficult to conceptualize, processing errors made at any of these stages will propagate through to the final product. Furthermore, when dealing with systematic LAI mapping over large extents of time and space, such as Canada-wide scenes throughout the growing season, site or overpass specific measurements of surface structure or reflectances and atmospheric properties are usually not available. In this research, we use existing algorithms published in Fernandes et al. (in press) for all LAI retrievals since the focus of this paper is strictly to measure the consistency (precision) with which remote LAI can be measured and not on LAI algorithm improvement (accuracy).

1.1 Atmospheric influence on LAI retrieval

The starting point for a systematic approach of LAI retrieval using remote sensing data is in the ability to accurately convert the information received at the satellite sensor to surface reflectance. The information received at the sensor not only includes measurements of reflected solar energy, but is inherently influenced by such factors as the sun-object-sensor angular relationship, the bi-directional reflectance distribution function (BRDF) of the surface being sensed, the spectral band response functions and the atmospheric properties at the time of sensor overpass. Such factors can profoundly affect the spatial or temporal analysis of remote sensing data and their influence should be quantified or at least acknowledged in any remote sensing study. Of special consideration in this research, is the influence of atmospheric correction on estimated

surface reflectance and the propagation of uncertainties in atmospheric correction to LAI retrieval.

Atmospheric scattering and absorption contributes to at-sensor radiance across all visible and infrared spectral bands on the TM sensor. Scattering of solar irradiance by atmospheric molecules and aerosols generates path radiance, which adds overall brightness to the scene under investigation. Local scattering at the pixel level is also common in a scene where neighbouring pixels over a heterogeneous surface contribute a portion of the reflected brightness into the path of the observed pixel. This effect (termed adjacency effect) tends to make the reflectance of dark pixels appear brighter, while bright pixels appear darker. Aerosols and other molecules in the atmosphere also absorb radiation that is reflected from the Earth's surface causing an overall loss of brightness to the scene as recorded by the satellite sensor. Both atmospheric scatter and absorption are enhanced at shorter wavelengths as aerosol particle sizes approach the spectral wavelength being recorded by the instrument and are dependent on the surface features under examination. Since many commercial satellite sensors offer unique spectral windows to minimize the influence of atmospheric molecular scattering and gas absorption on the recorded signal, the most common atmospheric correction procedures attempt to quantify the optical properties of the atmosphere at the time of the sensor overpass and apply radiative transfer algorithms to estimate surface bi-directional reflectance from at-sensor radiance.

An ideal method for quantifying atmospheric optical properties would be to obtain in-situ measurements in tandem with the sensor overpass (Thome, 2001). It is well documented that aerosol optical depth (AOD) is one of the most influential parameters in the atmospheric correction procedure for TM visible and infrared bands of land (Kaufman and Remer, 1994). However, due to the large variability in aerosol distributions both temporally and spatially (Liang et al., 2001), surface measurements can be difficult to acquire or may not be economically feasible in a research budget. Although, permanent atmospheric measurement stations have been established by the AERONET network (Holben et al., 1998), the distribution of these data over Canadian

landscapes (provided by the AERONET affiliate, AEROCAN) is spatially sparse and inadequate to systematically correct for Landsat atmospheric conditions in a consistent manner. Furthermore, AERONET data are also insufficient to quantify within scene aerosol variability.

Given such limitations, many researchers have derived methods to calculate atmospheric optical properties solely from the remotely sensed scene under investigation (Kaufman and Sendra, 1988). Current image processing methods to estimate aerosol concentrations use either: Invariant-Object Methods (Moran et al., 1992), Histogram Matching (PCI Inc., 2000), Dark Target Methods including dense, dark vegetation (Kaufman and Sendra, 1988; Teillet and Fedosejevs, 1995) or Contrast Reduction Methods (Tanre and Legrand, 1991). All are summarized in (Liang et al., 2001) and well-documented elsewhere for a variety of moderate (Santer et al., 1999; Lin et al., 2002) and high spatial resolution satellite sensors (Kaufman et al., 1997; Liu and Vermote, 2000). The dense, dark vegetation (DDV) approach was utilized in this study for its relative acceptance in the remote sensing community, for its usefulness in TM retrievals of aerosols over land (King et al, 1999;Liang et al., 1997), for its computational efficiency (Richter, 1996; Fallah-Adl et al., 1997) and lastly, for the successful validation that such an approach provides with accurate ancillary data from in-situ monitoring stations (Kaufman et al., 1993; Kaufman et al., 1997).

Given the importance of atmospheric conditions during satellite sensor overpass, the propagation of this uncertainty into LAI retrievals can be decomposed into bias and random errors due to both the algorithm applied and the vegetation index (VI) used as input to the algorithm. The LAI algorithms used here are empirical regressions between LAI and spectral vegetation indices derived from Landsat surface reflectances co-located over a number of calibration sites across Canada (Fernandes et al.). Our study focuses on differences in LAI due to uncertainties in calibration and atmospheric correction of the

vegetation indices required as input to the selected retrieval algorithms. This is of importance for two reasons:

(i) simulation studies suggest typical reflectance estimation errors of over 20% in retrieval of visible band reflectances for cloud free conditions due to uncertainties in current image based atmospheric correction algorithms (Knapp et al., 1999).

(ii) a model based sensitivity analysis of vegetation index retrieval uncertainty as a function of modest absolute uncertainties in aerosol optical depth at 550nm (AOD550) of +/- 0.10 suggests VI precision errors range from 15% to over 50% depending on surface conditions and VI used (Fernandes et al.).

A quantitative assessment of the actual uncertainty in LAI due to uncertainties in atmospheric correction is essential before a representative error budget can be derived for image based LAI products. Again, we limit our treatment to existing LAI algorithms developed at Canada Centre for Remote Sensing (Fernandes et al., 2003). By using overlapping TM data, we assume negligible change in surface reflectance, LAI and sensor radiometry. Thus differences between the two coincident regions are assumed to be predominantly due to changes in:

(a) Atmospheric condition
(b) Bi-directional reflectance function (BRF)
(c) Co-registration

To assess (a), we test four atmospheric correction techniques, comparing the consistency in LAI retrieval of each method. In general, (b) should be considered when comparing images acquired under different illumination and observation angles. However, no BRF adjustments were performed in this study, as the solar zenith angles were quite similar (maximum difference between overlap pairs was 3j) and the relative azimuth angles do not vary substantially from one Landsat overpass to another. The largest BRF effect would be the sensor viewing geometries, as they varied in the extreme cases by <F4.5j away from nadir. However, testing of this influence on coniferous forest canopies using two different models, the Walthall (Walthall, Norman, Welles, Campbell,

& Blad, 1985) and NTAM (Latifovic, Cihlar, & Chen, in press) resulted in maximum absolute surface reflectance differences of F0.005 for ETM+ band 3 (TM3) and <F0.002 for bands 4 (TM4) and 5 (TM5). For simplicity, any reference to a specific spectral band will be numerically noted after the TM acronym. To minimize the influence of (c) on LAI retrieval, one scene from each pair was co-registered to the companion scene and each overlap scene was spatially aggregated to a 90-m footprint. In summary, the research questions examined in this study were:

(1) What is the consistency in surface reflectance using a baseline atmospheric correction approach from Landsat ETM+ imagery?

(2) (2) What is the consistency in LAI retrieval when propagated from (1) for each atmospheric correction method?

2. Data and materials

2.1. Landsat scene selection

The 20 full Landsat ETM+ scenes used in this study are listed in Table 1 and their locations within Canada are displayed graphically in Figure 1 superimposed over a colour composite acquired from SPOT4-VEGETATION (VGT). The inset in the top right corner of Figure 1 illustrates a typical pair of LAI maps and the overlap region common to both (highlighted in white). The Landsat images were chosen based on (1) mid-summer overlap coverage over vegetated areas (particularly over forests and agriculture) during the summer growing season, (2) coverage with minimal cloud/ haze contribution, and (3) coverage south of the treeline where the existing LAI algorithms have been validated. We assume changes in surface conditions were negligible between scenes as the sensor imaged the overlap regions from 7 to 25 days apart. Available meteorological data was used to confirm an absence of precipitation for a 24-h period before each satellite image acquisition.

Table 1 – Landsat ETM+ scene selection. All overlap regions were imaged from 7 to 25 days apart.

WEST			EAST			ECOZONE
Path	Row	Date	Path	Row	Date	
14	28	June 8,2001	13	28	June 1,2001	Mixedwood Plains
22	24	July 15,2000	21	24	August 9,2000	Hudson Plains
22	26	July 5,2002	21	26	June 28,2002	Boreal Shield
24	22	July 29,2000	23	22	July 22,2000	Hudson Plains
28	24	August 26,2000	27	24	September 4,2000	Boreal Shield
32	22	July 21,2000	31	22	July 14,2000	Boreal Shield
34	20	July 3,2000	33	20	June 10,2000	Taiga Shield
39	24	July 20,1999	38	24	July 29,1999	Prairies
41	23	August 3,1999	40	23	July 27,1999	Boreal Plains
41	24	August 3,1999	40	24	July 27,1999	Prairies

The Landsat ETM+ data corresponded to Level 1G at-sensor-radiance systematically corrected and processed using the PGS processor by Radarsat International (RSI, Richmond, Canada). Sensor radiometric calibration was performed using the calibration gain and offset information provided in Landsat ETM+ header files.
The western image of each scene pair was geo-referenced to Lambert Conformal Conic projection (LCC, 49jN and 77jN as standard parallels, 95jWas the reference meridian) using nearest-neighbor, first-order transformations from the geographic coordinates provided in the header files together with vector coverages from the Canadian National Topographic Database (NTDB, Geomatics Canada, 1996). These scenes provided the base images to which all adjacent eastern scenes were co-registered using image-to image registration. In all cases, a minimum of eight ground control points were selected in each overlap region yielding an average root-mean-square error (RMSE) of less than 0.5 pixels (15 m).

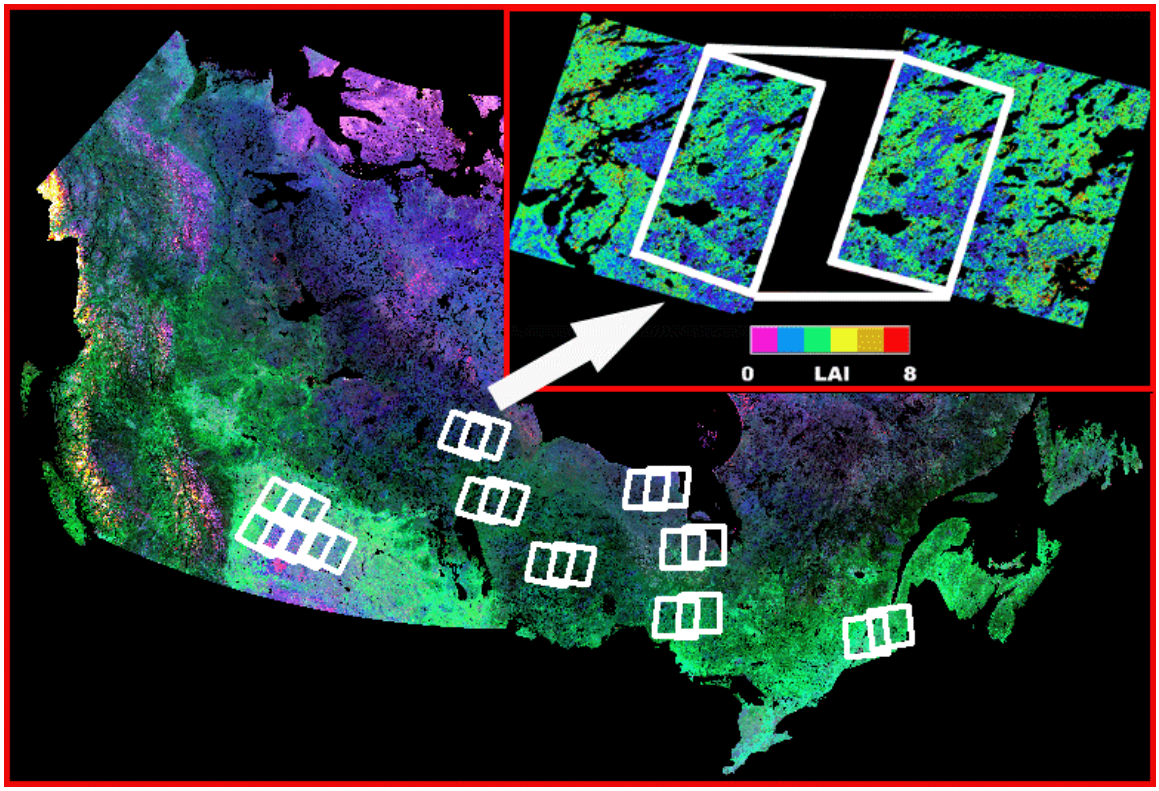

Figure 1 – Canada-wide colour composite from SPOT4-VEGETATION (VGT) with Landsat ETM+ scene locations in white. Inset shows LAI maps for 33/20 and 34/20 and the overlap region common to both.

2.2. Atmospheric correction: four correction methods

This section describes the four atmospheric correction procedures applied in this study. All methods incorporated scene-specific input parameters such as centre location coordinates, acquisition date and time along with the generic mid-latitude summer atmosphere and continental aerosol model inputs into the 6S radiative transfer code (Vermote, Tanre, Deuze´, Herman, & Morcrette, 1997). Elevation data for each scene was obtained from the NTDB at a scale of 1:100,000. The first two atmospheric correction methods incorporated a fixed aerosol concentration value whereas methods three and four evaluated scene-dependent aerosols. To test the influence of AOD550 on surface reflectance and LAI retrieval, method #1 applied a constant AOD550 with scene specific geographic information to each scene in the conversion from at-sensor radiance to surface reflectance. This method (herein referred to as the baseline method) was used

to test the assumption that there was no change in atmospheric conditions between the two overlap dates taking into account that there was a certain level of aerosols present in each of the two overlap scenes. Such an approach is often used as a standard approach for correction of Advanced Very High Resolution Radiometer (AVHRR) data and hence could serve as a starting point for Landsat ETM+ atmospheric correction (Cihlar et al., 2002). For this method, an AOD550 value of 0.06 was chosen to be representative of the typical aerosol contribution to remotely sensed data over the Canadian landmass as suggested by Ahern et al. (1991) and Fedosejevs et al. (2000).

The second atmospheric correction procedure was based on a no-correction scenario (referred herein as no-correction method). In this case, it was assumed that the atmosphere did not influence the satellite measurements. Surface reflectance was calculated from top-of-atmosphere directional reflectance in all overlap regions using a fixed aerosol optical depth at 550 nm (AOD550) equal to 0. The reflectance data from each scene were subsequently used in LAI retrieval.

The third atmospheric correction method incorporated the dense, dark vegetation approach to approximate a scene-dependent AOD550 with scene-specific geographic information. This method (referred to as the DDV correction) tested the assumption that the dense, dark vegetation approach would systematically identify and correct for changes in atmospheric conditions between acquisition dates. The DDV approach used in our atmospheric correction of satellite data used information extracted from selected DDV pixels across all spectral wavelengths in a scene to determine the contribution of path radiance influencing the pixel radiances recorded at the satellite sensor. The approach described here is similar to the methodology applied by Liang et al. (2001) with several modifications that were found to be more appropriate for Canadian landscapes. Dense, dark vegetation targets were defined from Landsat ETM+ band 7 (TM7) and a Normalized Difference Vegetation Index (NDVI) map as suggested by Kaufman and Tanre (1998) and Liang et al. (2001). A top-of-atmosphere TM7 threshold of 0.01–0.05 was used as a legitimate value of DDV reflectance since aerosols modestly affect this spectral region (2090–2350 nm). The TM7 range has been used in other DDV studies involving Landsat TM data (Quaidrari & Vermote, 1999; Song, Woodcock, Seto,

Lenney, & Macomber, 2001) and was assumed to be valid for all of the ETM+ data processed in this project. To demarcate dark vegetation targets, an NDVI>90th percentile was used as a threshold value.

Finally, the last atmospheric correction procedure used in this study, was based on AOD550 measurements obtained from the Moderate Resolution Imaging Spectroradiometer (MODIS) onboard the Terra (EOS AM) satellite. The method (herewith in referred to as the MODIS correction) was applied to test an alternative variable AOD550 correction methodology with our DDV approach described in the preceding section. MOD04_L2 granules representing geographic locations coincident with four ETM+ scene overpasses were obtained from NASA's Goodard Space Flight Center (GSFC) in the standard Hierarchical Data Format (HDF) (online: http://daac.gsfc.nasa.gov/data/dataset/ MODIS/02_Atmosphere/01_Level_2/01_Aerosol_Prod/ 2000/index.html).

Only the corrected optical depth parameter at 550 nm was utilized from each HDF file. To obtain this parameter, the ETM+ latitude and longitude scene centre position was located on each MOD04_L2 grid and the data from a 20_20 pixel square area (where it was assumed 1 pixel = 10 km at nadir) was extracted from the HDF file. Negative data values were dropped from further analysis (as these represent either no data pixels, or pixels processed using the ocean DDV algorithm) and the remaining data was averaged and calibrated using the appropriate slope and intercept coefficients (Chu, Personal communication). Due to data availability constraints for MODIS AOD550 measurements prior to the year 2001, only scenes for 2001 and 2002 could be processed using this methodology. This operation was performed for all four Landsat scenes during these 2 years, and the resultant AOD550 was applied with scene-specific geometry to the 6S radiative transfer code to obtain the atmospheric correction coefficients to convert top-of-atmosphere directional reflectance into surface reflectance.

3. Methods

The following section presents the methods used to assess the consistency inherent in the surface reflectance and LAI retrievals. This section has been organized into two subsections. The first subsection describes each of the consistency trials while the second subsection presents the methods used to retrieve LAI from the ETM+ scene.

3.1. Consistency trials

This analysis has been organized into two trials based on the research questions presented in Section 1.1. The first trial (trial #1) examines the situation where the atmosphere is assumed to remain unchanged in each overlap region between the two acquisition dates. For this trial, surface reflectance was obtained using the baseline atmospheric correction procedure. The results from this trial quantify the surface reflectance consistency to answer the first research question. The second trial (trial #2) compared the LAI retrieval differences for the baseline correction procedure in trial #1 and three different atmospheric correction scenarios. For this trial, surface reflectance was determined using a no correction scenario; the DDV atmospheric correction procedure and an atmospheric correction method using MODIS-derived AOD550 input estimates. These reflectance values were then used to generate LAI fields in order to assess the consistency of LAI retrieval. The results from this trial answer the second research question.

3.2. LAI retrieval

To model LAI from ETM+ surface reflectance measurements, each Landsat scene was initially processed using the Infrared Simple Ratio (ISR = TM4/TM5) LAI algorithm introduced by Fernandes et al. (2003) stratified using a 1- km spatial resolution land cover layer (Cihlar, Beaubien, & Latifovic, 2001) and a land use layer (Kerr & Cihlar, 2003) derived from SPOT4-VEGETATION (VGT). The LAI for pixels classified as needle-leaf forest was modeled using regression Eq. (1) while those pixels classified as broadleaf forest used Eq. (2).

$$LAI = (0.9000 + 0.6900 \ln ISR)^4 \quad (1)$$

$$LAI = (-0.3500 + 1.1200 ISR^{0.5})^4 \quad (2)$$

The regions defined as agriculture in the land cover map were modeled based on crop type from the land use map using either the Simple Ratio (SR) vegetation index or the NDVI due to the lack of field data to calibrate ISR-based regressions (for agriculture prediction equations refer to Table 2 in Fernandes et al., 2003). The scenes were co-registered into similar spatial domains, and the region of overlap was cropped into a new database. To minimize co-registration errors, a 3_3 moving average filter was used to degrade each of the overlap regions to a 90-m footprint. To assess the LAI consistency using the ISR algorithm within the overlap regions, the root mean square difference (RMSD) and relative absolute difference (RAD) were calculated on a per-pixel basis between the western and eastern overlap images, using the former as the reference.

4. Results

The results have been organized based on the structure of the research questions defined in Section 1.1. For simplicity, only the western scene from each overlap pair is listed in all tables.

4.1. Consistency analysis of surface reflectance retrieval using a baseline atmospheric correction

As shown in Table 2, the average surface reflectance retrieval differences for the 10 overlap regions range from 9% to 73% based on spectral reflectance factors between 0.055 and 0.251. TM1 produced the largest mean relative absolute difference of 73%, or an absolute reflectance difference of F0.055 between overlap regions. The mean reflectance in TM1 was slightly higher than found in Wang et al. (2001); however, the mean relative error fell within the bounds described by Vermote (2000). A maximum mean reflectance factor of 0.12 and a RAD of 126% were determined for TM1 in the overlap region between scenes 31/22 and 32/22. TM2 showed an average RAD of 47% for a mean absolute reflectance of 0.066. In this case, the overlap region between scenes 27/24 and 28/24 revealed the maximum RAD of 94% for a mean reflectance factor of 0.033. This difference seems unusually large especially over forest pixels as Vermote suggests < 12% uncertainty for this spectral band. TM3 produced an average RMSD of F0.18, or 32% RAD for a mean absolute reflectance of 0.055. In this spectral band, the

scenes dominated by agriculture produced the largest absolute reflectance factors (0.078–0.103) and subsequently the lowest relative errors (13–20%). The smallest reflectance retrieval differences were derived for TM4, where the absolute reflectance could be F0.025 for a mean reflectance factor of 0.25. This result is consistent with Wang et al. (2001); however, the needleleaf- dominated scenes (33/20, 34/20 and 27/24, 28/24) usually underestimated the vegetation reflectance in this band. TM5 produced slightly larger differences than TM4. An average RAD of 12% was calculated for 10 samples, where the highest difference of 15% was noticed in the overlap region between scenes 38/24 and 39/24 and also between scenes 33/20 and 34/20. TM7 showed an average RAD equal to 18% for a mean absolute reflectance of 0.083. The overlap region between scenes 13/28 and 14/ 28 was responsible for the maximum RAD in this spectral band.

Table 2
Surface reflectance consistency for Landsat TM overlap regions derived from the baseline atmospheric correction
Band Spectral range (nm)

Band	Spectral range (nm)	Mean REF	Mean RMSD	Max RMSD	Range RMSD	Mean RAD	Max RAD	Range RAD
1	450– 515	0.063	0.055	0.091	0.083	73	126	107
2	525– 605	0.066	0.033	0.056	0.047	47	94	86
3	630– 690	0.055	0.018	0.03	0.023	32	67	54
4	750– 900	0.251	0.025	0.043	0.029	9	16	10
5	1550– 1750	0.153	0.019	0.039	0.03	12	15	8
7	2090– 2350	0.083	0.019	0.04	0.035	18	28	16

‘‘Mean REF’’ refers to the mean surface reflectance factor, RMSD refers to the root-mean-square-difference and RAD refers to the relative absolute difference
as a percentage of the mean reflectance factor.

4.2. Consistency in LAI retrieval when propagated from baseline corrected surface reflectance

Table 3 presents the LAI retrieval differences under the baseline atmospheric correction procedure. The mean LAI value for all land cover types in each overlap pair is shown along with the derived RMSD in LAI units and RAD as a percentage of the mean. Overall, mean LAI values < 2 units tend to occur in overlap regions located in the Prairie, Taiga shield or Hudson plains ecozones. In these regions, grasslands or agriculture are

the dominant land cover type. Larger LAI values (>2 units) occur in forest-dominated cover types.

As shown in Table 3, the baseline atmospheric correction procedure produced an average LAI root mean square difference of 0.61, or 26% of a mean LAI of 2.05 units. The overlap region between scenes 33/20 and 34/20 presented the largest relative difference of 61% for a mean LAI of 1.13 units. The smallest relative difference was calculated for the overlap region between scenes 21/24 and 22/24. The RAD for this overlap region was 14% for a mean LAI of 1.98 units. Seven of the ten overlap sets processed fell below the mean relative difference of 26% revealing a skewed distribution characterized by a standard deviation in RAD of 14%. Two overlap sets having resultant RAD values above the mean were dominated by agricultural land cover and produced mean LAI values c0.8 units. Since the overlap region between 40/23 and 41/23 is located one World Reference System (WRS) row north of the former two scenes, it contains more forested land cover types, is less likely to change between overlap acquisition dates, and produced a substantially smaller RAD of 17% for a mean LAI of 2.29 units.

Table 3
LAI retrieval consistency, root mean square difference (RMSD) and relative absolute difference (RAD) derived from the overlap analysis of baseline atmospherically corrected reflectance data

Path	Row	Mean LAI	RMSD (LAI)	RAD (%LAI)	Sample size (pixels)
39	24	0.81	0.40	39	238386
41	23	2.29	0.57	17	229200
41	24	0.79	0.57	29	353615
34	20	1.13	0.61	61	424600
32	22	2.21	0.59	19	371185
22	24	1.98	0.49	14	451032
24	22	1.38	0.35	16	309968
28	24	3.12	0.95	23	454848
14	28	3.14	0.87	24	430278
22	26	3.62	0.70	19	294600
	Mean	2.05	0.61	26	
	S.D.	1.02	0.19	14	

Figure 2 presents histograms of the LAI residual differences obtained for the baseline atmospheric correction scenario. The histograms have been divided into Figure

2a and b for display purposes. The largest residual differences were observed between scenes 27/24 and 28/24 (shown as the circle symbol in Figure 2b) with a mean difference of _0.4 LAI units and scenes 21/26 and 22/26 (shown as the pointed star in Figure 2b) with a mean difference of + 0.5 LAI units. A negative LAI residual in the overlap region reveals that a larger LAI occurred in the western overlap scene whereas a positive residual shows the opposite. Thus, the overlap regions for scenes 28/24 and 21/26 showed larger mean LAI values than their overlap counterparts. The majority of scenes (7 of 10) had residual differences ranging from F0.25 LAI units. While this may indicate that the baseline correction scenario will provide consistent results over a given region, the relatively large scatter in residuals shown in Figure 2b (e.g. one standard deviation confidence interval ranging from 0.35 LAI to 0.90 LAI in the dramatic cases) suggests that there is an additional random error component occurring between overpasses. It is unlikely that this is due to changes in measured LAI (or reflectance) caused by surface moisture differences given that the imagery was acquired at least 24 h away from a precipitation event and that a large area of drying or wetting should show up as a second mode in the residual histogram.

Although 24 h may not be sufficient to rule out any moisture differences present in the overlap areas as soil moisture does not vary much from one day to the next in this region, another explanation could be the presence of phenological changes in the overlap area between acquisition dates. While this could be true for scenes 33/20 and 34/ 20 (23 days apart) having the largest RAD (61%), it is certainly not true for scenes 21/24 and 22/24 (25 days apart), which yielded the lowest RAD (14%). Furthermore, to address the assumption of no phenological differences between the two acquisition dates, an analysis segmenting forest from agriculture RMSD and RAD values was performed. Only 4 of 10 overlap pairs contained both agriculture and forest pixels and three of these characterized lower RMSD and RAD values for agriculture LAI. The overlap pair 38/24–39/24 had the largest difference in RMSD values for forest and agriculture of 0.85 and 0.38, respectively. In this region, forest pixels were limited to woodland, low-density deciduous or treed barren land cover types where LAI differences may be largely dependent on the combination of understory and overstory vegetation phenology changes. This situation may also exist in the overlap regions for scenes 40/23–41/23 and

40/24–41/24 where similar results were obtained. The overlap region for scenes 13/28–14/28 presented a forest RMSD of 0.82 units while the agriculture RMSD was 0.97. In this case, the number of forest and agriculture pixels was evenly distributed, leading to relatively high overall mean LAI of 3.14 units. It is unclear at this point why the agriculture RMSD for this overlap pair is double the value obtained for the other scenes having agriculture pixels; however, this presents something that warrants further investigation.

A third explanation is that the baseline atmospheric correction procedure failed to quantify atmospheric differences between overlapping pairs or the within-scene spatial variability in atmospheric conditions. The influence of this spatial variability in AOD550 was not addressed in this study for lack of validation data; however, the influence of between-scene AOD550 variability was tested in the second trial of this study.

4.3. LAI retrieval consistency comparison for two other atmospheric correction methods and a no correction scenario

The results from trial #2 are illustrated in Tables 4 and 5. Table 4 shows the LAI differences derived for the no correction method, whereas Table 5 presents the LAI differences calculated for the DDV atmospheric correction.

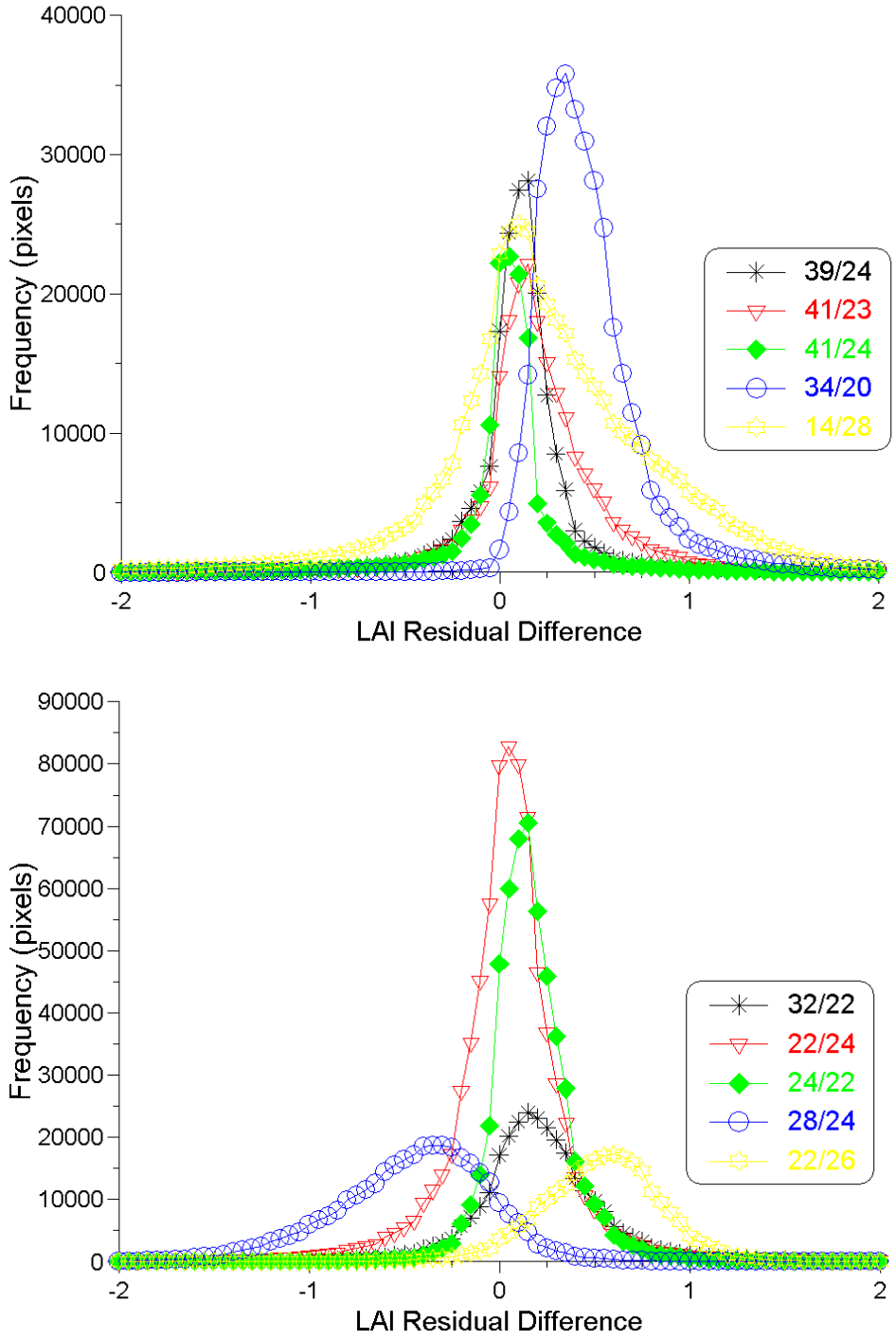

Figure 2 - Histograms illustrating the residual placement of differences for each set of overlap scenes for the baseline atmospheric correction procedure. The figure was divided into parts a. and b. for display purposes.

4.3.1. No atmospheric correction

Table 4 presents the results of the second trial using the no correction approach to derive LAI consistency in the overlap regions. In this analysis, a mean RMSD of 0.59 LAI units and mean RAD of 25% was calculated over 10 samples. The RAD was improved by 1% on average from the baseline method, which indicates that a bias exists when converting from top-of-atmosphere reflectance to surface reflectance using constant, though different AOD550 values. This bias is minimized as AOD550 concentrations are lower which is characterized in the comparison of results between the no correction and baseline correction methods. The mean LAI for all scenes was 1.97 units.

Table 4 – LAI retrieval consistency, root mean square difference (RMSD) and relative absolute difference (RAD) derived from the overlap analysis of LAI derived using top-of-atmosphere surface reflectance data. Values in braces ({}) represent the percent change from the baseline atmospheric correction method.

Path	Row	Mean LAI	RMSD (LAI)	RAD (% LAI) {% change from baseline}
39	24	0.65	0.36	37{-2}
41	23	1.74	0.49	15{-2}
41	24	0.76	0.55	**29{0}**
34	20	1.17	0.60	57{-4}
32	22	2.23	0.60	**19{0}**
22	24	2.01	0.51	15{+1}
24	22	1.41	0.37	**16{0}**
28	24	3.22	0.96	22{-1}
14	28	2.93	0.77	22{-2}
22	26	3.61	0.70	18{-1}
	Mean	1.97	0.59	25{-1}
	St. Dev.	1.02	0.18	13{-1}

Three of the ten overlap regions tested showed a 2% decrease in LAI retrieval difference over the baseline atmospheric correction method, while another three showed a modest 1% decrease. The scenes shown in bold font in Table 4 showed zero change from the baseline scenario meaning that the atmospheric contribution to these differences was

undetectable in this analysis. The overlap region between scenes 28/24 and 27/24, located in the boreal forest of northern Ontario, characterized the largest RMSD of 0.96 LAI units; however, due to the higher LAI values here, the RAD was 3% below the mean value for this trial and 1% below the baseline atmospheric correction approach. Such a difference may be influenced by end-of-season changes in LAI between the two acquisition dates of August 26 and September 3. The overlap region between scenes 34/20 and 33/20 produced the highest relative difference for this trial of 57% for a mean LAI of 1.17 units; however, this was improved by 4% over the RAD derived under the baseline method.

4.3.2. DDV atmospheric correction

Table 5 presents the range of differences calculated for the DDV atmospheric correction scenario, which differ substantially from those derived from the baseline correction method.

The largest change (+ 6%) was noticed in scenes 38/24 and 39/24 over the baseline correction scenario. For this pair, the RMSD more than doubled from 0.40 LAI units to 0.89 LAI units. Such a large difference in this case may be caused by the highly variable reflectance values for dense, dark vegetation in agricultural areas thus producing large values of AOD550. In this scene, many of the DDV targets fell on crop fields consisting of very high NDVI values (mean >0.9), relatively high TM3 reflectance factors (mean = 7.5%) and low TM7 reflectance (mean = 4.5%). Furthermore, the AOD550 values derived for the east and west scenes were very high, measured at 0.79 and 0.89, respectively. This was not the case in other scenes containing lesser agricultural land and more forest or grassland cover (e.g. 41/23 and 41/24). The DDV algorithm derived quite similar and lower AODs for these scenes except for the 40/24 and 41/24 image pair. The overlap region for this pair derived an LAI retrieval difference of 30%, representing a 1% increase from the baseline correction method even though the calculated values for AOD550 were very different between scenes (0.74 and 0.39, respectively). The three scenes highlighted in bold in Table 5 show either 0 or _1% change in derived LAI consistency from the baseline correction procedure. When processing these scenes, the systematic LAI retrieval differences are the same (or improved by 1%) when the DDV

atmospheric correction is applied over the baseline correction method. For all 10 scenes, the consistency differences derived for the DDV atmospheric correction procedure were approximately 29% for a mean LAI of 2.32, which is 2% larger than those calculated for the baseline correction scenario.

4.3.3. MODIS atmospheric correction

The LAI differences derived from the overlap analysis of MODIS atmospherically corrected reflectance data were very similar to the results derived from the DDV correction trial. Due to limitations on data availability, only four scenes, representing two overlap regions were processed in this analysis. Although this is a preliminary assessment of the integration of MODIS-derived aerosol products into a Landsat ETM+ data processing chain, future work should include such data integration. In both cases, the RAD increased by 1% over the baseline correction method.

Path	Row	Mean LAI	RMSD (LAI)	RAD (% LAI)
				{% change from baseline}
39	24	1.91	0.89	45{+6}
41	23	3.51	0.79	18{+1}
41	24	0.88	0.66	30{+1}
34	20	1.19	0.65	65{+4}
32	22	2.33	0.65	21{+2}
22	24	1.99	0.59	19{+5}
24	22	1.39	0.35	**16{0}**
28	24	3.16	1.14	27{+4}
14	28	3.20	0.90	**23{-1}**
22	26	3.62	0.68	**18{-1}**
	Mean	2.32	0.73	28{+2}
	St. Dev.	1.00	0.21	16{+2}

Table 5 – LAI retrieval consistency, root mean square difference (RMSD) and relative absolute difference (RAD) derived from the overlap analysis of DDV atmospherically corrected reflectance data. Values in braces ({}) represent the RAD change from the baseline atmospheric correction method.

Although the RMSD values decreased slightly from the DDV correction results for scenes 13/28 and 14/28, when compared to Table 5 there is no difference in RAD for these two processing methods.

5. Discussion

The consistency in surface reflectance using a baseline atmospheric correction was tested in the first trial of this study. Across 10 overlap samples, TM1 and TM2 showed the largest relative differences of 73% and 47%, respectively. This was expected since both spectral bands are very dependent on the atmospheric conditions at the time of sensor overpass. TM4 characterized the smallest average relative difference of 9%, whereas TM3 had an average RAD of 32%. TM5 showed a slightly larger RAD than TM4, while the average RAD obtained for TM7 was twice as large as that recorded for TM4. At longer spectral wavelengths, the increase in relative absolute difference may have been due to water vapour absorption differences between scenes. Testing of this parameter across all scenes resulted in an average difference in absolute surface reflectance factor of 0.05 in TM7 using water vapour values of 2.93 and 5.0 g/cm2.

This consistency was then propagated to LAI retrieval in order to answer the second research question addressed in this study. LAI differences obtained for 10 samples was calculated on average to be F0.61 LAI units or 26% relative absolute difference. Seven out of ten samples had residual differences ranging from _0.25 to + 0.25 LAI units. The other samples produced a larger residual scatter, which may have been caused by local atmospheric contamination due to haze or the generic atmospheric correction procedure incorporated into this specific trial. In this trial, the maximum RAD of 61% that occurred between scenes 33/20 and 34/20 was likely caused by (1) different atmosphere components or (2) changing land surface between acquisition dates. In this case, the difference in acquisition dates was 23 days in June and July during the peak time for seasonal leaf growth (Chen, 1995). Thus, either (or both) of these issues could be causing the high retrieval differences.

To examine the second research question, the influence of various atmospheric correction procedures on LAI retrieval was evaluated. In this case, LAI retrieval differences were compared for two other atmospheric correction methods and a no

correction scenario to the baseline correction. The DDV correction assumed the atmosphere to be variable between acquisition dates and attempted to quantify this change using dark targets collected at the ETM+ scale (30 m).

In this analysis, the no correction approach performed better in terms of consistency (_1%, RAD), than both the DDV correction scenario (+ 2%, RAD) and the baseline correction procedure. The MODIS correction, similar to the DDV correction, assumed variable atmospheric contributions to surface reflectance estimates and quantified these changes based on dark targets collected at the MODIS (500 m) spatial resolution. Although the analysis incorporated only two samples, this correction performed equally well when compared to the DDV correction procedure used at the ETM+ 30 m scale. Even though this result is promising, future work should address the advantages of integrating MODIS-derived atmospheric products in the correction of Landsat imagery. Although the DDV correction approaches resulted in less consistent estimates of LAI, future testing will assess the absolute accuracy of LAI retrieval, as it is expected to improve over the baseline or no correction scenarios. This is important in order to link satellite-based reflectance and LAI retrieval models to actual measurements made in situ. In applications where absolute quantities are required for example, the DDV atmospheric correction method should provide more reliable estimates over the no correction scenario, a method that carries an unrealistic assumption of no atmospheric contamination in satellite based remote sensing applications. The lower consistency obtained using the DDV approaches may have also been caused by limitations in the methodology used to derived DDV targets. For instance, gas absorption affects the retrieval of AOD from the DDV approach. Take for example the water absorption in TM7, which determines the surface reflectance in the TM3 channel. Without a water vapour correction, the TM7 will be underestimated, and the resultant AOD will be overestimated. This issue will be the focus of future work since we used fixed values of water vapour and ozone in all of the atmospheric correction procedures and obtained average reflectance factor differences of 18%. Furthermore, the DDV aerosol concentrations used in this study were only measured in the troposphere and did not account for the vertical AOD distribution in the stratosphere. Lastly, future work should also consider the spatial variability of aerosols

within a Landsat scene and how these influence retrieval consistency of LAI and other biophysical parameters measured from satellite imagery.

6. Conclusions

In this study, a consistency analysis of systematic surface reflectance and leaf area index retrieval was performed using overlap regions in adjacent Landsat scenes. For all 20 Landsat scenes analyzed, it was assumed the land surface reflectance and land use remained constant between acquisition dates. Each Landsat ETM+ scene was independently co-registered and corrected for atmospheric effects in a number of different sensitivity trials. Empirical LAI models were then applied to the surface reflectance data and the LAI difference in the overlap region of each image pair was evaluated. The results from this analysis show that systematic LAI retrieval from Landsat ETM+ imagery using a baseline atmospheric correction approach is consistent to within F0.61 LAI units. The average relative difference in LAI retrieval for 10 image pairs was 26% for a mean LAI of 2.05 and the maximum relative difference was determined to be 61% for a mean LAI of 1.13. For all 10 overlapping samples, different atmospheric correction methods produced variable results. When no atmospheric correction was performed on the data, the LAI retrieval consistency was improved by 1%. When a Landsat-based dense, dark vegetation atmospheric correction algorithm was used, the LAI retrieval differences became 2% worse. Using a subset of only 2 overlapping samples, a MODIS derived DDV atmospheric correction produced similar results to the Landsat based DDV correction. Although the DDV correction methods produce lower consistency than the baseline approach when applied to clear-sky imagery, they still represent a realistic approach for capturing and quantifying atmospheric conditions in a systematic and repeatable procedure for obtaining biophysical quantities. This is an important point since it is known that the atmosphere changes the reflected energy recorded at the satellite sensor; however, the magnitude of change (absolute) is always scene-dependent and is usually not accounted for in quantitative terms. Conversely, for use in relative change detection applications or simple qualitative studies, the no correction or baseline atmospheric correction procedures may be more beneficial to implement.

The ultimate test of performance for systematic LAI maps are comparison to ground truth. However, this is challenging when dealing with data sets spanning large spatial and temporal extents. Our study tested an important aspect of surface reflectance and LAI retrieval from Landsat imagery by quantifying differences due to atmospheric correction uncertainties related to AOD specification. Such differences are considered to be over and above any differences due to BRDF effects induced by substantial topography found in mountainous regions. Again, we identified two levels of testing:

(1) Sensitivity analysis of image-based atmospheric correction algorithms.
(2) Consistency analysis of image-based LAI retrieval.

The first approach is commonly used but the idea of consistency analysis has not often been applied outside categorical map comparison (e.g. Guindon & Edmonds, 2001). An added benefit of consistency analysis is that it can provide a good estimate of background noise levels for studies that rely on relative changes in LAI rather than absolute LAI estimates (Hall et al., 2003). The results formulated in this study will progress future work aimed towards LAI retrieval from fine and moderate spatial resolution sensors especially over disturbances, changing phenology, areas of substantial relief, and very wet or dry regions.

Acknowledgements

We would like to acknowledge Sylvain Leblanc, Phillip Teillet, Robert Landry, Frank Ahern, and Wenjun Chen for comments, information and material support to carry out this work. Thank you to the internal reviewer at CCRS for providing a careful and timely review of the manuscript prior to submission.

References

Ahern, F. J., Gauthier, R. P., Teillet, P. M., Sirois, J., Fedosejevs, G., & Lorente, D. (1991). An investigation of continental aerosols with high resolution solar extinction measurements. Applied Optics, 30, 5276– 5287.

Bonan, G. B. (1995). Land–atmospheric interactions for climate system models: Coupling biophysical, biogeochemical and ecosystem dynamical processes. Remote Sensing of Environment, 51, 57– 73.

Cayrol, P., Chehbouni, A., Kergoat, L., Dedieu, G., Mordelet, P., & Nouvellon, Y. (2000). Grassland modeling and monitoring with SPOT-4 VEGETATION instrument during the 1997–1999 SALSA experiment. Agricultural and Forest Meteorology, 105, 91– 115.

Chen, J. M. (1995). Optically-based methods for measuring seasonal variation of leaf area index in Boreal Forest conifer stands. Agricultural and Forest Meteorology, 80, 135– 163.

Chen, J. M., Pavlic, G., Brown, L., Cihlar, J., Leblanc, S. G., White, H. P., Hall, R. J., Peddle, D., King, D. J., Trofymow, J. A., Swift, E., Van der Sanden, J., & Pellikka, P. (2002). Validation of Canada-wide leaf area index maps using ground measurements and high and moderate resolution satellite imagery. Remote Sensing of Environment, 80, 165– 184.

Chu, A. (Personal communication). MODIS Aerosol Team Principal Investigator contacted on October 24, 2002 at achu@climate.gsfc. nasa.gov regarding scale and offset coefficients for Corrected_Optical_ Depth_Land parameter.

Cihlar, J., Beaubien, J., & Latifovic, R. (2001). Land cover of Canada 1998. Digital data set documentation. Ottawa, Ontario: Natural Resources Canada.

Cihlar, J., Chen, J., Li, Z., Latifovic, R., Fedosejevs, G., Adair, M., Park,W., Fraser, R., Trishchenko, A., Guindon, B., Stanley, D., & Morse, D. (2002). GeoComp-n, an advanced system for the processing of coarse and medium resolution satellite data: Part 2. Biophysical products for Northern Ecosystems. Canadian Journal of Remote Sensing, 28, 21– 44.

Cohen, W. B., & Justice, C. O. (1999). Validating MODIS terrestrial ecology products: Linking in situ and satellite measurements. Remote Sensing of Environment, 70, 1–4.

Coops, N. C., Waring, R. H., & Landsberg, J. J. (2001). Estimation of potential forest productivity across the Oregon transect using satellite data and monthly weather records. International Journal of Remote Sensing, 22, 3797– 3812.

Fallah-Adl, H., JaJa, J., & Liang, S. (1997). Fast algorithms for estimating aerosol optical depth and correcting Thematic Mapper (TM) imagery. Journal of Supercomputing, 10, 315– 330.

Fedosejevs, G., O'Neill, N. T., Royer, A., Teillet, P. M., Bokoye, A. I., & McArthur, L. J. B. (2000). Aerosol optical depth for atmosheric correction

of AVHRR composite data. Canadian Journal of Remote Sensing, 26, 273– 284.
Fernandes, R., Butson, C., Leblanc, S. G., & Latifovic, R. (2003). A Landsat TM/ETM+ based accuracy assessment of leaf area index products for Canada derived from SPOT4/VGT data. Canadian Journal of Remote Sensing, 29(2), 241– 258.
Geomatics Canada, (1996). Standards and specifications of the National Topographic Database Edition 3.18. Sherbrooke, Que, Canada: Minister of Supply and Services Canada (CATALOGUE NO M52-70/1996).
Goodchild, M. (2000). Communicating the results of accuracy assessment. Metadata, digital libraries and assessing fitness for use. In H. T. Mowrer, & R. G. Congalton (Eds.), Quantifying spatial uncertainty in natural resources (pp. 3 – 15). Chelsea, MI, USA: Ann Arbor Sci. Publ.
Guindon, B., & Edmonds, C. M. (2001). Exploiting inter-scene overlap to improve large area land cover mapping from Landsat imagery. 2001 ASPRS Annual Conference, St. Louis, MO, April 23– 27.
Hall, R. J., Fernandes, R. A., Hogg, E. H., Brandt, J. P., Butson, C. R., Case, B. S., & LeBlanc, S. G. (2003). Relating aspen defoliation to changes in leaf area derived from field and satellite remote sensing data. Canadian Journal of Remote Sensing, 29(3), 299– 313 (Special Issue on LAI).
Holben, B. N., Eck, T. F., Slutsker, I., Tanre´, D., Buis, P. J., Setzer, A., Vermote, E., Reagan, J. A., Kaufman, Y. J., Nakajima, T., Lavenu, F., Jankowiak, I., & Smirnov, A. (1998). AERONET—a federated instrument network and data archive for aerosol characterization. Remote Sensing of Environment, 66, 1– 16.
Houser, P., & Cosgrove, B. (2002). LDAS—Land Data Assimilation System' web site: (http://ldas.gsfc.nasa.gov/) published by NASA, USA accessed April 20, 2002.
Kaufman, Y. J. (1993). Aerosol optical thickness and atmospheric path radiance. Journal of Geophysical Research, 98, 2677–2692.
Kaufman, Y. J., & Remer, L. A. (1994). Detection of forests using mid-IR reflectance: An application for aerosol studies. IEEE Transactions on Geoscience and Remote Sensing, 32, 672– 683.
Kaufman, Y. J., & Sendra, C. (1988). Algorithm for automatic atmospheric corrections to visible and near-IR satellite imagery. International Journal of Remote Sensing, 9, 1357–1381.
Kaufman, Y. J., & Tanre, D. (1998). Algorithm for remote sensing of tropospheric aerosol from MODIS. ATDB reference number ATBD-MOD-02. Washington-DC, USA: Goodard Space Flight Centre-NASA (Online distribution: http://ltpwww.gsfc.nasa.gov/MODIS-Atmosphere/ _docs/atbd_mod02.pdf).
Kaufman, Y. J., Wald, A. E., Remer, L. A., Gao, B., Li, R., & Flynn, L. (1997). The MODIS 2.1-Am channel—correlation with visible reflectance for use in remote sensing of aerosol. IEEE Transactions on Geoscience and Remote Sensing, 35, 1286– 1297.

Kerr, J. T., & Cihlar, J. (2003). Land use and cover with intensity of agriculture for Canada from satellite and census data. Global Ecology and Biogeography, 12, 161– 172.
King, M. D., Kaufman, Y. J., Tanre, D., & Nakajima, T. (1999). Remote sensing of tropospheric aerosols from space: Past, present and future. Bulletin of the American Meteorological Society, 80, 2229–2259.
Knapp, K. R., Vonder Haar, T. H., & Kaufmann, Y. J. (1999). Aerosol optical property retrievals: The effect of surface reflectance uncertainty. Proceedings of the 10th Atmospheric Conference on Radiation, Madison, Wisconsin, July, 1999. (pp. 304–307). Boston, MA, USA: American Meteorological Society.
Latifovic, R., Cihlar, J., & Chen, J. (2003 January). A comparison of BRDF models for the normalization of satellite optical data to a standard sun– target – sensor geometry. IEEE Transactions on Geoscience and Remote Sensing.
Liang, S., Fallah-Adl, H., Kalluri, H., Jaja, J., Kaufman, Y. J., & Townshend, R. G. (1997). An operational atmospheric correction algorithm for Landsat Thematic Mapper imagery over the land. Journal of Geophysical Research, 102, 17173–17186.
Liang, S., Fang, H., & Chen, M. (2001). Atmospheric correction of Landsat ETM+ Land Surface Imagery: Part 1. Methods. IEEE Transactions on Geoscience and Remote Sensing, 39, 2490– 2498.
Lin, T. H., Chen, A. J., Liu, G. R., & Kuo, T. H. (2002). Monitoring the atmospheric aerosol optical depth with SPOT data in complex terrain. International Journal of Remote Sensing, 23, 647– 659.
Liu, C. H., & Vermote, E. (2000). A reflectance retrieval algorithm for Landsat TM satellite image. Pathumthani, Thailand: Asia Centre for Research and Remote Sensing (Online distribution at: http://www. gisdevelopment.net/aars/acrs/2000/ts9/imgp0019.shtml).
Liu, J., Chen, J. M., Cihlar, J., & Park, B. (1997). A process-based boreal ecosystem productivity simulator using remote sensing inputs. Remote Sensing of Environment, 62, 158–175.
Marriott, F. H. C. (1990). A dictionary of statistical terms. (5th ed.). Chelsea, MI, USA: Longman. 223 pp.
Moran, S. M., Jackson, R. D., Slater, P. N., & Teillet, P. M. (1992). Evaluation of simplified procedures for retrieval of land surface reflectance factors from satellite sensor output. Remote Sensing of Environment, 41, 169– 184.
Mowrer, H. T., & Congalton, R. G. (2000). Introduction: The past, present and future of spatial uncertainty analysis. In H. T. Mowrer, & R. G. Congalton (Eds.), Quantifying spatial uncertainty in natural resources (pp. xv– xxiv). Chelsea, MI, USA: Ann Arbor Sci. Publ.
Myneni, R. B., Nemani, R. R., & Running, S. W. (1997). Algorithm for the estimation of global land cover, LAI and FPAR based on radiative transfer models. IEEE Transactions on Geoscience and Remote Sensing, 35, 1380–1393.

Nouvellon, Y., Rambal, S., Lo Seen, D., Moran, M. S., Lhomme, J. P., Be´gue´, A., Chehbouni, A. G., & Kerr, Y. (2000). Modelling of daily fluxes of water and carbon from shortgrass steppes. Agricultural and Forest Meteorology, 100, 137–153.
PCI-EASI Software Package. Version 7—released June 2000.
Quaidrari, H., & Vermote, E. F. (1999). Operational atmospheric correction of Landsat TM data. Remote Sensing of Environment, 70, 4– 15.
Richter, R. (1996). A spatially adaptive fast atmospheric correction algorithm. International Journal of Remote Sensing, 17, 1201–1214.
Santer, R., Carrere, V., Dubuisson, P., & Roger, J. C. (1999). Atmospheric correction over land for MERIS. International Journal of Remote Sensing, 20, 1819–1840.
Sellers, P. J., Los, S. O., Tucker, C. J., Justice, C. O., Dazlich, D. A., Collatz, G. J., & Randall, D. A. (1994). A global 1j by 1j NDVI data set for climatic studies: Part 2. The adjustment of the NDVI and generation of global fields of terrestrial biophysical parameters. International Journal of Remote Sensing, 17, 3519–3546.
Song, C., Woodcock, C. E., Seto, K. C., Lenney, M. P., & Macomber, S. A. (2001). Classification and change detection using Landsat TM data: When and how to correct atmospheric effects? Remote Sensing of Environment, 75, 230–244.
Su, Z. (2000). Remote sensing of land use and vegetation for mesoscale hydrological studies. International Journal of Remote Sensing, 21, 213– 233.
Tanre, D., & Legrand, M. (1991). On the satellite retrieval of Saharan dust optical thickness over land: Two different approaches. Journal of Geophysical Research, 96, 5221–5227.
Teillet, P. M., & Fedosejevs, G. (1995). On the dark target approach to atmospheric correction of remotely sensed data. Canadian Journal of Remote Sensing, 21, 374– 388.
Thome, K. (2001). Absolute radiometric calibration of Landsat 7 ETM+ using the reflectance-based method. Remote Sensing of Environment, 78, 27– 38.
United Nations FAO. Online distribution: http://www.fao.org/gtos/tems/variables/Leaf_area_index.pdf. Accessed February 2002.
Vermote, E. (2000). Product accuracy/uncertainty: MOD09, surface reflectance, atmospheric correction algorithm product. MODIS data products catalog (EOS AM Platform) (Available at: http://modarch.gsfc.nasa.gov/MODIS/RESULTS/DATAPROD/).
Vermote, E. F., Tanre, D., Deuze´, J. L., Herman, M., & Morcrette, J. J. (1997). Second simulation of the satellite signal in the solar spectrum, 6S: An overview. IEEE Transactions on Geoscience and Remote Sensing, 35, 675– 686.
Walthall, C. L., Norman, J. M., Welles, J. M., Campbell, G., & Blad, B. L. (1985). Simple equation to approximate the bi-directional reflectance from vegetative canopies and bare soil surfaces. Applied Optics, 24,

383– 387.
Wang, Y., Tian, Y., Zhang, Y., El-Saleous, N., Knyazikhin, Y., Vermote, E., & Myneni, R. (2001). Investigation of product accuracy as a function of input and model uncertainties case study with SeaWiFS and MODIS LAI/FPAR algorithm. Remote Sensing of Environment, 78, 299– 313.
Waring, R. H., & Running, S. W. (1998). Forest ecosystems analysis at multiple scales. (2nd ed.). Seattle, WA: Academic Press.
Wood, J. E., Gillis, M. D., Goodenough, D. G., Hall, R. J., & Leckie, D. G. (2002). Earth Observation for Sustainable Development of forests (EOSD): Project overview. Proceedings of the 24th Symposium on Geoscience and Remote Sensing, IGARSS, June 24– 28 2002.